RSC Advances

PAPER

View Article Online
View Journal | View Issue

Cite this: *RSC Adv.*, 2019, **9**, 39604

The photogenerated charge characteristics in Ni@NiO/CdS hybrids for increased photocatalytic H_2 generation†

Lijing Zhang,*[b] Xiufang Zhu,*[b] Yuanyuan Zhao,[b] Pengyu Zhang,[b] Jing Chen,[b] Jinlong Jiang[b] and Tengfeng Xie*[a]

Received 3rd August 2019
Accepted 4th November 2019

DOI: 10.1039/c9ra06034k

rsc.li/rsc-advances

Solar-driven H_2 generation from water splitting with semiconductor materials is considered an effective solution to solve the problems of energy shortage and environmental pollution at a low cost. In this study, a highly efficient photocatalyst Ni@NiO/CdS for H_2 evolution was synthesised using a simple solvothermal method and calcination. The HRTEM results and elemental mapping tests confirmed that Ni@NiO was successfully loaded on the surface of CdS. For Ni@NiO loaded, Ni@NiO/CdS exhibited remarkable photocatalytic H_2 evolution activity of 87.6 μmol h^{-1}, which was about 104 times higher than that of pure CdS. The enhanced H_2 evolution activity of Ni@NiO/CdS was ascribed to the prolonged lifetime of the photogenerated charges and the reduced surface overpotential for H_2 evolution.

1. Introduction

Solar-driven H_2 generation from water splitting is an attractive and promising technique.[1–5] Semiconductor-based photocatalysts play an important role in photocatalytic H_2 generation from water splitting. For example, graphitic carbon nitride is an effective photocatalyst for H_2 evolution.[6–8] CdS, which absorbs visible light because of its narrow band gap, has a more negative potential for the reduction of H^+ to H_2; therefore, it is considered as a promising material for H_2 evolution from water splitting.[9,10] Jiang *et al.* reported that the photocatalytic H_2 evolution rate of CdS with 3 wt% MoS_2 was as high as 11.4 mmol h^{-1} g^{-1}.[11] However, pure CdS shows low H_2 generation efficiency because most photogenerated charges recombine before reducing H^+ to H_2. Therefore, to improve the photocatalytic H_2 generation efficiency, a cocatalyst is essential for CdS. Noble metals, such as platinum, are outstanding cocatalysts for photocatalytic H_2 evolution; however, these metals are expensive, have very limited availability and cannot be used in large-scale applications.[12,13] Therefore, the development of cocatalysts based on non-noble metals is necessary to realize highly efficient and stable photocatalytic H_2 evolution.

Recently, transition metals, such as Fe, Co, Ni, and Mo-based cocatalysts, have received considerable attention because of their low cost and high efficiency.[14–17] Currently, most studies on transition metal cocatalysts focus on ameliorating the separation efficiency of photogenerated charges or reducing the surface overpotential for hydrogen evolution. There are very few studies on non-noble metals, which can not only obviously increase the charge separation efficiency, but also reduce the surface overpotential. The research team of Professor Nørskov in Denmark found that the Gibbs free energy of Ni in non-noble metals is the closest to zero. Therefore, among the non-noble metals, Ni is the most suitable for H_2 evolution.[18] However, the photocatalytic H_2 efficiency of Ni as a cocatalyst is low because of its high overpotential for H_2 evolution.[19] Recently, the research team of Professor Shuhong Yu in the University of Science and Technology of China reported that a large number of defective states in NiO can weaken the H–O bond in H_2O, which can effectively accelerate the dissociation of water.[20] The research team of Professor Hongjie Dai in Stanford University found that NiO can effectively reduce the overpotential of electrocatalytic hydrogen evolution.[21] After NiO is loaded, the overpotential for electrocatalytic hydrogen evolution can even be reduced to 0 mV. Moreover, Dai *et al.* speculated that NiO as a cocatalyst can absorb hydroxyl radicals from the decomposition of water, which is beneficial as Ni can absorb hydrogen and reduce hydrogen atoms. However, the actual reason for the role of NiO as a cocatalyst is still unclear.

In this study, we synthesized Ni@NiO/CdS using a simple solvothermal method and calcination. A schematic diagram of the synthesis of the Ni@NiO/CdS photocatalyst is shown in Scheme 1, which reflects the synthetic process of the photocatalyst. The HRTEM results and elemental mapping tests

[a]State Key Laboratory of Theoretical and Computational Chemistry, College of Chemistry, Jilin University, Changchun 130012, China. E-mail: xietf@jlu.edu.cn
[b]College of Chemical Engineering, National & Local Joint Engineering Research Center for Mineral Salt Deep Utilization, Key Laboratory for Palygorskite Science and Applied Technology of Jiangsu Province, Huaiyin Institute of Technology, Huaian 223003, China. E-mail: lijingz16@hyit.edu.cn; xiufangzhu@hyit.edu.cn

† Electronic supplementary information (ESI) available. See DOI: 10.1039/c9ra06034k

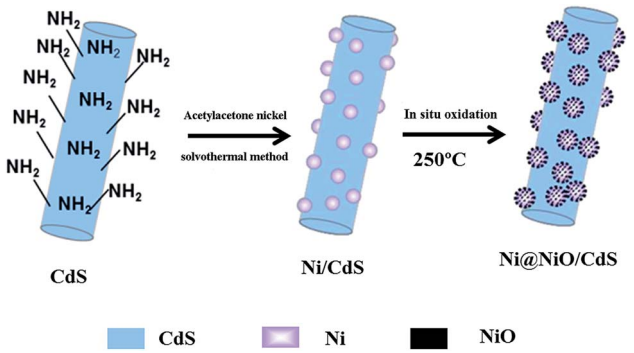

Scheme 1 Schematic diagram of the synthesis of Ni@NiO/CdS photocatalyst.

confirmed that Ni@NiO was successfully loaded on the surface of CdS. Also, the photocatalytic activity of CdS was considerably enhanced by the Ni@NiO cocatalyst. To explore the reason for the enhancement in photocatalytic H_2 evolution activity by Ni@NiO cocatalyst, the photogenerated charge characteristics of Ni@NiO/CdS were examined using surface photovoltage (SPV) measurements.

2. Experimental

2.1 Material synthesis

2.1.1 Synthesis of cadmium sulfide. We used the solvothermal method to synthesize CdS nanorods. According to a previously reported procedure, cadmium nitrate tetrahydrate ($Cd(NO_3)_2 \cdot 4H_2O$) was used as the cadmium source and thiourea (NH_2CSNH_2) was used as the sulfur source, and ethylenediamine was used as the solvent. The reaction was conducted for 48 h at 160 °C.

2.1.2 Synthesis of Ni@NiO/CdS. We synthesized a composite of Ni metal and CdS using the solvothermal method. We dispersed some nickel acetyl acetone in 30 mL of *N*,*N*-dimethylformamide (DMF) with stirring. Then, some of the obtained CdS nanorods were added to the above solution. The mixture was sonicated for 10 min at room temperature. Then, the mixture was transferred to a 100 mL Teflon-lined autoclave, sealed and heated at 200 °C for 10 h. The black product was obtained by centrifugation, washed with ethanol several times, and dried at 50 °C for 10 h under vacuum. Finally, the as-obtained Ni/CdS was calcined at 250 °C for 1 h to obtain the Ni@NiO/CdS product. For comparison, the CdS nanorods were also treated with DMF at 200 °C and 10 h without nickel acetyl acetone.

2.2 Material characterization

The sample morphologies were studied using an XL 30 ESEM FEG field-emission scanning electron microscope (FESEM; FEI Company). X-ray diffraction patterns were obtained by scanning the sample in the 2θ range of 20° and 80° at a scanning rate of 10° min^{-1} using a Rigaku D/Max-2550 diffractometer with Cu-K_α radiation (λ = 1.54056 Å; 40 kV, 350 mA). UV-vis diffuse reflectance spectra (UV-vis DRS) of the samples were obtained using a UV-vis-NIR spectrophotometer (Shimadzu UV-3600) in the absorption range of 300 to 800 nm. Transmission electron microscopy (TEM) and high-resolution transmission electron microscopy (HRTEM) images were obtained using a TECNAIG2 TEM microscope (FEI Company). X-ray photoelectron spectra (XPS) of the Ni@NiO/CdS samples were obtained using a Thermo VG Scientific Escalab 250 spectrometer. Furthermore, the photoinduced charge characteristics of Ni@NiO/CdS were studied *via* SPV and transient photoelectronic voltage (TPV) measurements on home-made instruments; moreover, the TPV instrument used a laser light as the illuminant. The light wavelength was 355 nm and the pulse width was 5 ns as the illuminant. Data storage was performed using a digital oscilloscope.

2.3 Photocatalytic reaction

We tested the photocatalytic H_2 evolution activity of Ni@NiO/CdS using a Quartz reactor. Note that the irradiating area was 5.3 cm^2. A 500 W Xe lamp was used to provide light. The catalyst mass was 20 mg and triethanolamine was used as the electronic donor. We used gas chromatography to test the amount of H_2 with a TOC detector and N_2 as the carrier gas.

3. Results and discussion

Fig. 1 displays a comparison of the XRD patterns of CdS, Ni, Ni@NiO, and Ni@NiO/CdS. As shown in Fig. 1, the diffraction peaks in the X-ray diffraction (XRD) spectrum of CdS can be attributed to the wurtzite phase of CdS [JCPDS no. 77-2306]. Moreover, peaks for a strong metallic Ni phase (JCPDS no. 45-1027 and 65-2865) can be detected for the Ni metal and Ni@NiO samples, whereas a peak for a weak NiO phase (JCPDS no. 47-1094) was observed for Ni@NiO. In fact, the wurtzite phase of CdS was also observed for Ni@NiO/CdS. Moreover, the peak at 44.5° for Ni@NiO/CdS is assigned to Ni; however, diffraction peaks belonging to NiO were not observed, possibly because of its poor crystallinity.

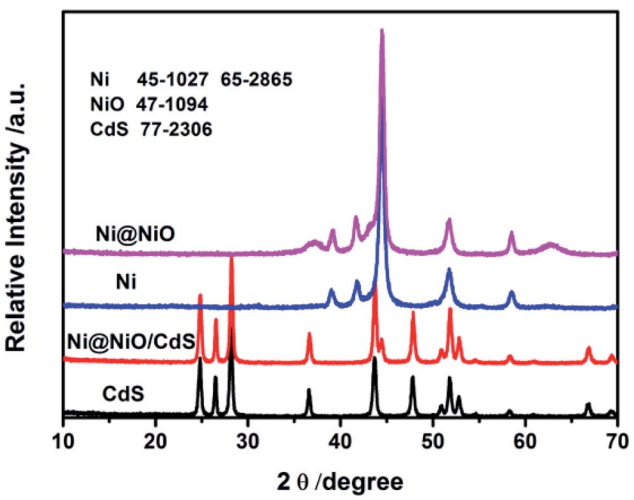

Fig. 1 XRD patterns of CdS, Ni, Ni@NiO and Ni@NiO/CdS.

Fig. 2 shows the FESEM images of CdS, Ni@NiO/CdS and Ni@NiO nanocomposites. As shown in Fig. 2(b), CdS exhibits a rod-likes structure. The diameter of the rods ranges from 30 to 50 nm, whereas the length of the rods ranges from 0.2 to 3 μm. Notably, the surface of the CdS nanorods is smooth (Fig. 2(b)) and the Ni@NiO/CdS nanocomposite shows a rod-like structure (Fig. 2(c)). However, compared with pure CdS, the surface of the Ni@NiO/CdS nanorods is rough and many small particles are present on the CdS nanorods (Fig. 2(d)). Furthermore, we obtained the free Ni@NiO core/shell NPs with a diameter of about 50–500 nm (Fig. 2(e and f)).

We used XPS measurement to further study the elemental composition of Ni@NiO/CdS and determine the valency of Ni element in Ni@NiO. Fig. 3 shows the XPS survey spectrum of Ni@NiO/CdS, in which the peaks of S 2p, Cd 3d, Ni 2p, O 1s and C 1s can be observed. The peaks of C can be attributed to CO_2 and adventitious hydrocarbon absorbed on Ni@NiO/CdS from the equipment.[22] The binding energy of Ni $2p_{1/2}$ and Ni $2p_{3/2}$ are 853.5 and 873.6 eV and the shake-up satellite peaks are observed at 861 and 879 eV, respectively, which indicate the presence of NiO (Fig. 3(b)).[23,24] Moreover, the binding energy of Ni $2p_{3/2}$ is 855.4 eV, which proves the existence of the $Ni(OH)_2$ phase or Ni_2O_3 phase. Because of the poor thermal stability of Ni_2O_3, the surface of NiO contains $Ni(OH)_2$ rather than Ni_2O_3.[25]

To obtain detailed information about the nanostructure and morphology of Ni@NiO/CdS, HRTEM imaging of Ni@NiO/CdS was performed, as shown in Fig. 4. From the TEM images shown in Fig. 4(a) and (c), it can be seen that the CdS surface is uniformly coated with many nanoparticles. Furthermore, the high-resolution TEM (HRTEM) images (Fig. 3(b)) show that the spacing of 0.11 nm corresponds to the (112) plane of Ni, whereas the spacing of 0.336 nm corresponds to the (002) plane of CdS. As can be seen in Fig. 4(d), elemental mapping reveals that the Ni element is evenly distributed on the Ni@NiO/CdS composite.

Fig. 5 shows the photocatalytic performance for hydrogen evolution on CdS, Ni/CdS, Ni@NiO/CdS, and Ni@NiO. In the absence of a catalyst, there was no clear increase in H_2, which indicates that the hydrogen evolution involves light catalysis. Pure CdS displayed a low photocatalytic hydrogen evolution rate in the presence of light. Because nanosized particles tend to aggregate and light-induced charges tend to recombine. The

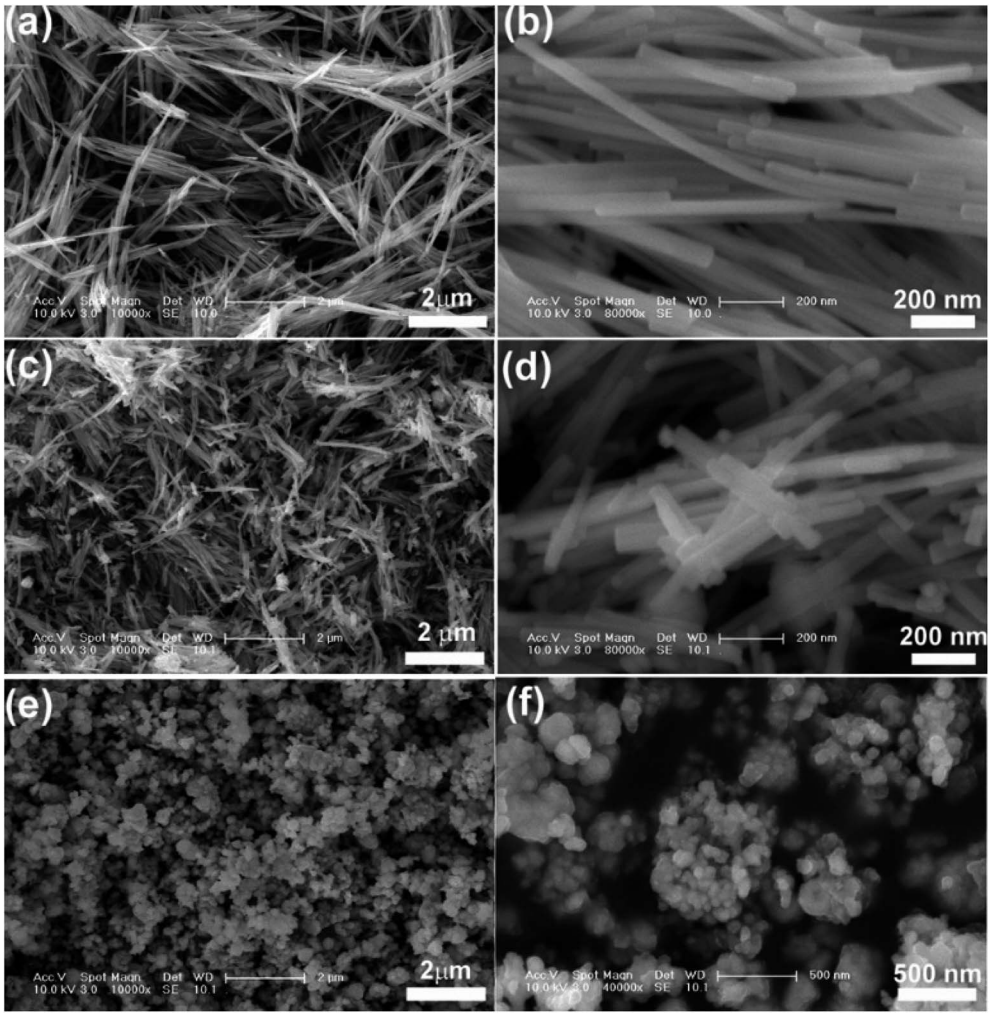

Fig. 2 (a and b) FESEM images of CdS, (c and d) FESEM images of Ni@NiO/CdS and (e and f) FESEM images of Ni@NiO.

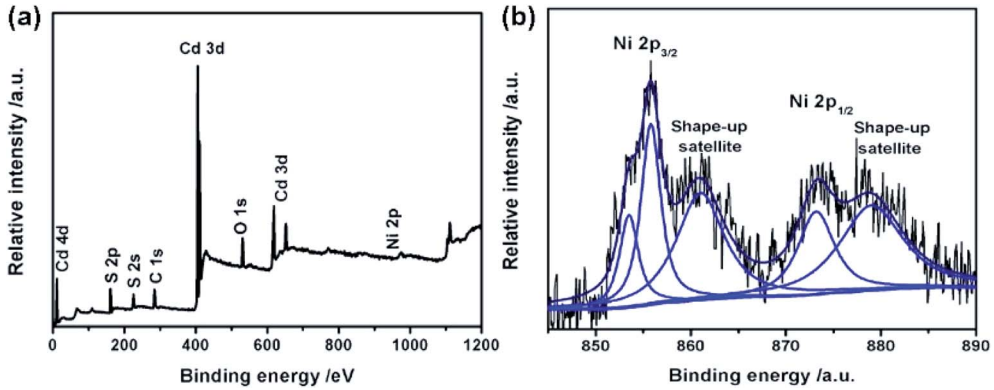

Fig. 3 XPS spectra of Ni@NiO/CdS: (a) survey spectrum and (b) Ni 2p region of the XPS spectrum.

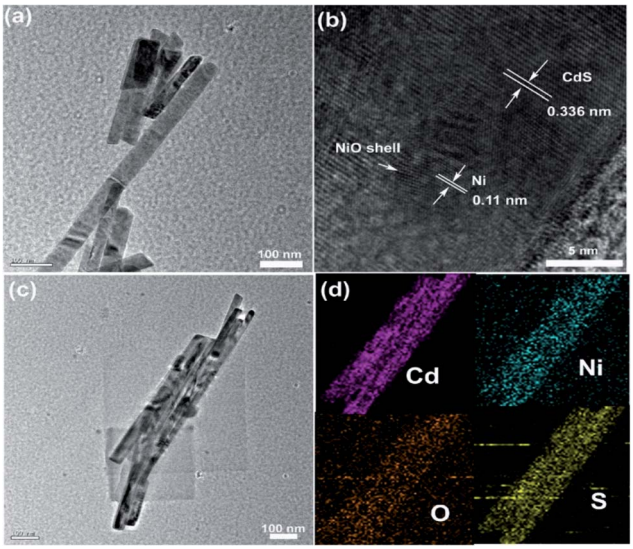

Fig. 4 HRTEM images of Ni@NiO/CdS: (a and c) TEM images of Ni@NiO/CdS, (b) high-resolution TEM images of Ni@NiO/CdS, and (d) elemental mapping images of Cd, Ni, O and S.

light-induced hydrogen evolution rate of CdS was significantly improved for the Ni-loaded. Moreover, Ni@NiO/CdS with NiO loaded on the surface of Ni, demonstrated the highest rate of 87.6 μmol h^{-1}. Note that only Ni@NiO exhibited no clear photocatalytic hydrogen evolution activity. Furthermore, the photocatalytic H_2 evolution rate of Ni@NiO/CdS is higher than that reported for $NiCoP/C_3N_4$,[26] CuS/CdS,[27] $CuS/Zn_{0.8}Cd_{0.2}S$ (ref. 28) and $CdS/Pt/WO_3$,[29] but is lower than that reported for MoS_2/CdS.[11] Although the test conditions such as light intensity, frequency and the type and amount of sacrificial agent used should be the same for a fairer comparison.

The SPV and TPV instruments were used to study the role of Ni@NiO on the surface of CdS in the photocatalytic H_2 evolution process of photocatalytic hydrogen generation by investigating the light-induced charges properties. Both techniques are considered very promising approaches for researching the dynamic characteristics of light-induced charges. Fig. 6 shows the SPV spectra of CdS, Ni/CdS, Ni@NiO/CdS and Ni@NiO. All the samples show a positive signal according to the band gap transition of CdS. It is a typical characteristic of n-type materials. The SPV response of Ni/CdS obviously decreased for the Ni-loaded composite. Fig. 7 shows the work function mapping measurements of CdS and Ni. According to the formula of W_f [eV] = $W_{f,Au}$ + ΔCPD/1000, the working function of Ni is larger than the working function of CdS. Therefore, when Ni is loaded

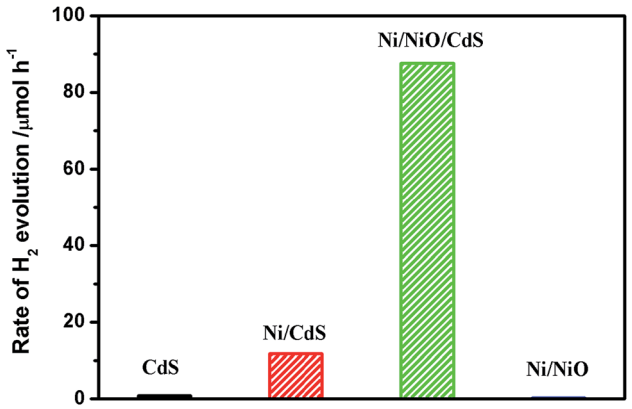

Fig. 5 Rate of H_2 evolution on CdS, Ni/CdS, Ni@NiO/CdS and Ni@NiO.

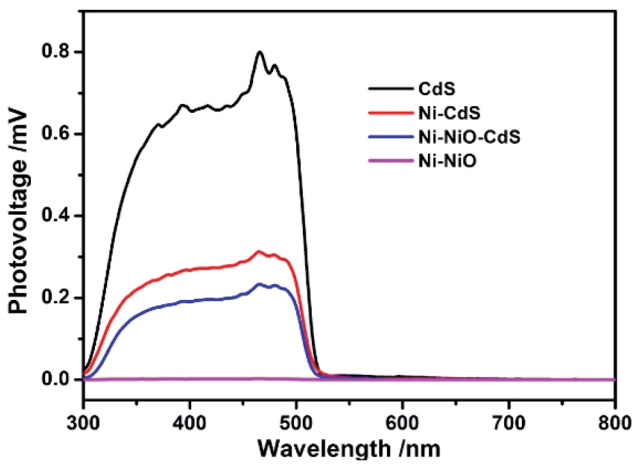

Fig. 6 SPS (surface photovoltage spectra) of CdS, Ni/CdS, Ni@NiO/CdS and Ni@NiO.

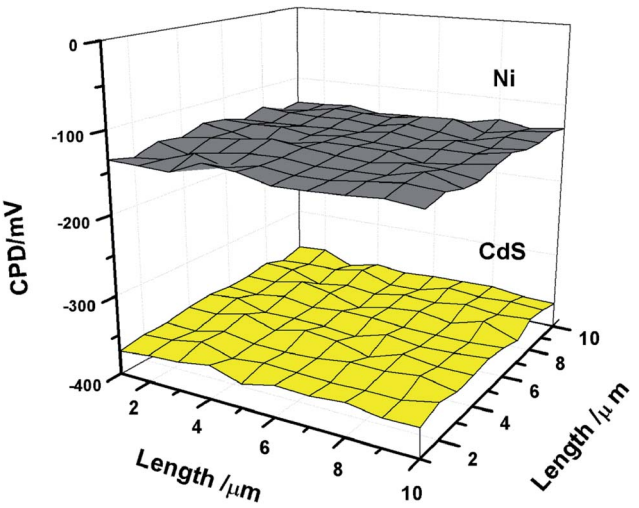

Fig. 7 Work function mapping measurements of CdS and Ni.

on CdS, it can capture electrons. Note that this can weaken the effect of the space-charge area of CdS, and NiO lowers the photovoltage signal further. However, an apparent photovoltage signal was not observed for Ni@NiO.

The dynamic characteristics of the photogenic charges of Ni@NiO/CdS were further studied using the TPV instrument. The transient photovoltage signal of CdS, Ni/CdS, and Ni@NiO/CdS with 355 nm laser light is shown in Fig. 8. As is known, a photoelectric signal is enhanced when light-generated electrons and holes are separated in the surface space charge area. Thus, dynamic information on light-induced electrons and holes in Ni@NiO/CdS, including their generation, separation and recombination, can be obtained from the TPV spectra. Accordingly, we estimated the time of for the whole separation and recombination process of photogenerated electron–hole pairs. Fig. 8 shows that compared with the TPV signal of CdS, the TPV signal moves toward the longer timescale for Ni/CdS and Ni@NiO/CdS. This indicates that Ni and Ni@NiO loaded on CdS decreased the recombination of light-induced charges in CdS and extended the photogenerated charge lifetime in CdS, which then resulted in higher photocatalytic H_2 evolution activity. Furthermore, because of the photogenerated electrons trapped by Ni and Ni@NiO, the time value for the P1 peak for Ni/CdS and Ni@NiO/CdS was shorter than that for the P1 peak of CdS.

Stability is a very important parameter to evaluate catalysts. Thus, a cycle experiment using Ni@NiO/CdS for photocatalytic H_2 evolution was conducted. Four cycles were tested, with each cycle lasting 4 h. Fig. S1† shows the photocatalytic H_2 activity of Ni@NiO/CdS in four cycles, where the photocatalytic H_2 activity of Ni@NiO/CdS decreased obviously with an increase in cycle number. Also, as the reaction progressed, we found that the color of the photocatalyst changed from black green to black. This can due to the photocorrosion of CdS and the instability of Ni@NiO. Therefore, the stability of the Ni@NiO/CdS composite photocatalyst needs to be improved.

Through the above analysis, we found that the photocatalytic H_2 evolution activity of Ni@NiO/CdS is obviously higher than that of Ni/CdS, while the photogenerated charge separation efficiency of Ni@NiO/CdS is slightly higher than that of Ni/CdS. Thus, improved photogenerated charge separation efficiency may be not the main reason for the further increase in the photocatalytic H_2 evolution rate of Ni@NiO/CdS. Thiel *et al.* proposed that NiO, which is rich in defect states, can dissociate adsorbed water molecules.[20,30,31] Dai *et al.* speculated that NiO can absorb hydroxyl radicals from the decomposition of water, which can create favorable conditions for the diffusion and reduction of H^+.[32] Therefore, we proposed the possible mechanism for photocatalytic H_2 evolution (Scheme 2). Under illumination, photogenerated electrons are separated from holes. Because the work function of Ni is greater than that of CdS, the photogenerated electrons are captured by Ni, which improve the charge separation efficiency. While, the main function of NiO on the surface is to weaken the H–O bond, absorb

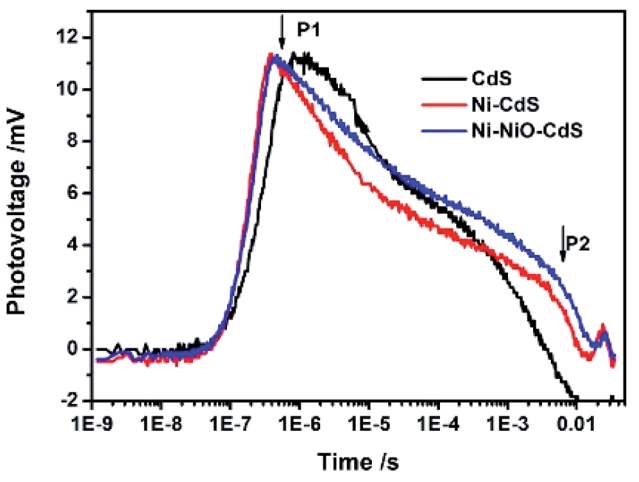

Fig. 8 TPV of CdS, Ni/CdS and Ni@NiO/CdS. The light wavelength was 355 nm and the pulse width was 5 ns.

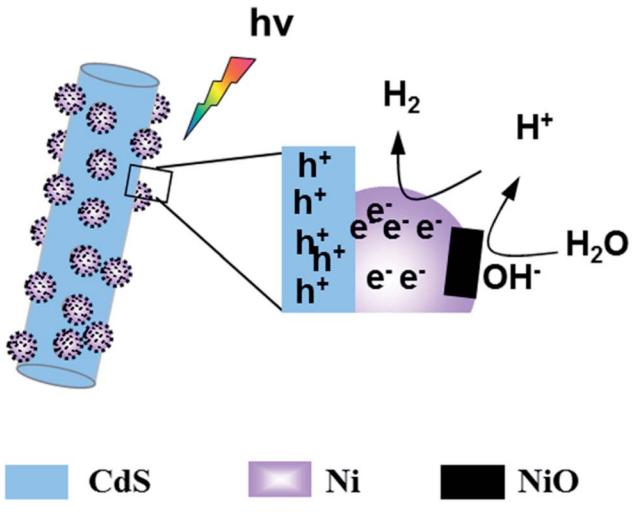

Scheme 2 Schematic diagram of photocatalytic H_2 evolution of Ni@NiO/CdS.

hydroxide, and accelerate the dissociation of water, which lead to a reduction in the overpotential for H_2 evolution. These two reasons lead to the increase in photocatalytic H_2 evolution activity.

4. Conclusion

In summary, we prepared Ni@NiO/CdS samples using a solvothermal and calcination method. The Ni@NiO/CdS sample showed the highest photocatalytic H_2 evolution activity of 87.6 μmol h^{-1}. Our results indicate that Ni acts an electron acceptor and effectively prolongs the photogenerated charge lifetime in CdS. While main function of NiO is to weaken the H–O bond, absorb hydroxide, and accelerate the dissociation of water, which lead to a reduction in the overpotential for H_2 evolution. The synergistic effect of Ni and NiO is the main reason for the excellent photocatalytic H_2 evolution activity of Ni@NiO/CdS.

Conflicts of interest

There are no conflict to declare.

Acknowledgements

For financial support, we are grateful to the National Science Youth Foundation of China (No. 51704123, No. 21602074 and No. 201605055), Provincial Science Youth Foundation of Jiangsu (No. BK20160424, No. BK20160425), National Natural Science Foundation of China (No. 51574130, No. 51572106 and No. 21773086) and Foundation of Key Laboratory for Palygorskite Science and Applied Technology of Jiangsu Province (201504 and 201505).

References

1 A. Naldoni, M. Altomare, G. Zoppellaro, *et al.*, Photocatalysis with Reduced TiO_2: From Black TiO_2 to Co-catalyst-free Hydrogen Production, *ACS Catal.*, 2018, **9**(1), 345–364.
2 K. C. Christoforidis and P. Fornasiero, Photocatalytic hydrogen production: a rift into the future energy supply, *ChemCatChem*, 2017, **9**(9), 1523–1544.
3 D. Spanu, S. Recchia, S. Mohajernia, *et al.*, Templated Dewetting–Alloying of NiCu Bilayers on TiO_2 Nanotubes Enables Efficient Noble-Metal-Free Photocatalytic H_2 Evolution, *ACS Catal.*, 2018, **8**(6), 5298–5305.
4 W. Liu, X. Wang, H. Yu, *et al.*, Direct Photoinduced Synthesis of Amorphous $CoMoS_x$ Cocatalyst and Its Improved Photocatalytic H_2-Evolution Activity of CdS, *ACS Sustainable Chem. Eng.*, 2018, **6**(9), 12436–12445.
5 D. J. Martin, K. Qiu, S. A. Shevlin, *et al.*, Highly efficient photocatalytic H_2 evolution from water using visible light and structure-controlled graphitic carbon nitride, *Angew. Chem., Int. Ed.*, 2014, **53**(35), 9240–9245.
6 Y. Guo, J. Li, Y. Yuan, *et al.*, A Rapid Microwave-Assisted Thermolysis Route to Highly Crystalline Carbon Nitrides for Efficient Hydrogen Generation, *Angew. Chem., Int. Ed.*, 2016, **55**(47), 14693–14697.
7 J. Li, D. Wu, J. Iocozzia, *et al.*, Achieving efficient incorporation of π-electrons into graphitic carbon nitride for markedly improved hydrogen generation, *Angew. Chem., Int. Ed.*, 2019, **58**, 1985–1989.
8 D. Wu, S. Hu, H. Xue, *et al.*, Protonation and microwave-assisted heating induced excitation of lone-pair electrons in graphitic carbon nitride for increased photocatalytic hydrogen generation, *J. Mater. Chem. A*, 2019, **7**(35), 20223–20228.
9 F. Q. Zhou, J. C. Fan, Q. J. Xu, *et al.*, $BiVO_4$ nanowires decorated with CdS nanoparticles as Z-scheme photocatalyst with enhanced H_2 generation, *Appl. Catal., B*, 2017, **201**, 77–83.
10 W. Zhong, W. Tu, S. Feng, *et al.*, Photocatalytic H_2 evolution on CdS nanoparticles by loading FeSe nanorods as co-catalyst under visible light irradiation, *J. Alloys Compd.*, 2019, **772**, 669–674.
11 L. Jiang, L. Wang, G. Xu, *et al.*, A microwave-assisted thermolysis route to single-step preparation of MoS_2/CdS composite photocatalysts for active hydrogen generation, *Sustainable Energy Fuels*, 2018, **2**(2), 430–435.
12 G. Zhao, Y. Sun, W. Zhou, *et al.*, Superior photocatalytic H_2 production with cocatalytic Co/Ni species anchored on sulfide semiconductor, *Adv. Mater.*, 2017, **29**(40), 1703258.
13 Z. Li, X. Chen, W. Shangguan, *et al.*, Prickly Ni_3S_2 nanowires modified CdS nanoparticles for highly enhanced visible-light photocatalytic H_2 production, *Int. J. Hydrogen Energy*, 2017, **42**(10), 6618–6626.
14 X. Lu, J. Xie, S. Liu, *et al.*, Low-Cost Ni_3B/$Ni(OH)_2$ as an ecofriendly hybrid cocatalyst for remarkably boosting photocatalytic H_2 production over g-C_3N_4 nanosheets, *ACS Sustainable Chem. Eng.*, 2018, **6**(10), 13140–13150.
15 Z. Mao, J. Chen, Y. Yang, *et al.*, Novel g-C_3N_4/CoO nanocomposites with significantly enhanced visible-light photocatalytic activity for H_2 evolution, *ACS Appl. Mater. Interfaces*, 2017, **9**(14), 12427–12435.
16 Y. Chao, J. Zheng, J. Chen, *et al.*, Highly efficient visible light-driven hydrogen production of precious metal-free hybrid photocatalyst: CdS@ NiMoS core–shell nanorods, *Catal. Sci. Technol.*, 2017, **7**(13), 2798–2804.
17 D. Spanu, S. Recchia, S. Mohajernia, *et al.*, Templated Dewetting–Alloying of NiCu Bilayers on TiO_2 Nanotubes Enables Efficient Noble-Metal-Free Photocatalytic H_2 Evolution, *ACS Catal.*, 2018, **8**(6), 5298–5305.
18 J. Greeley, T. F. Jaramillo, J. Bonde, *et al.*, Computational high-throughput screening of electrocatalytic materials for hydrogen evolution, *Nat. Mater.*, 2006, **5**(11), 909–913.
19 T. Simon, N. Bouchonville, M. J. Berr, *et al.*, Redox shuttle mechanism enhances photocatalytic H_2 generation on Ni-decorated CdS nanorods, *Nat. Mater.*, 2014, **13**(11), 1013.
20 Y. F. Xu, M. R. Gao, Y. R. Zheng, *et al.*, Nickel/nickel(II) oxide nanoparticles anchored onto cobalt(IV) diselenide nanobelts for the electrochemical production of hydrogen, *Angew. Chem.*, 2013, **125**(33), 8708–8712.
21 M. Gong, W. Zhou, M. C. Tsai, *et al.*, Nanoscale nickel oxide/nickel heterostructures for active hydrogen evolution electrocatalysis, *Nat. Commun.*, 2014, **5**(5), 4695.

22 J. Yu, Y. Hai and B. Cheng, Enhanced Photocatalytic H_2-Production Activity of TiO_2 by $Ni(OH)_2$ Cluster Modification, *J. Phys. Chem. C*, 2011, **115**, 4953–4958.

23 J. Moulder, W. Stickle, P. Sobol and K. Bomben, *Handbook of X-ray Photoelectron Spectroscopy*, Physical Electronics, Inc, Eden Prairie, MN, 1992, pp. 1–190.

24 K.-D. Kim, J. W. Nam, H. O. Seo, Y. D. Kim and D. C. Lim, Oxidation of Toluene on Bare and TiO_2-Covered NiO-$Ni(OH)_2$ Nanoparticles, *J. Phys. Chem. C*, 2011, **115**, 22954–22959.

25 M. T. Greiner, M. G. Helander, Z. B. Wang, W. M. Tang and Z. H. Lu, Effects of Processing Conditions on the Work Function and Energy-Level Alignment of NiO Thin Films, *J. Phys. Chem. C*, 2010, **114**, 19777–19781.

26 L. Bi, X. Gao, L. Zhang, *et al.*, Enhanced photocatalytic hydrogen evolution of NiCoP/g-C_3N_4 with improved separation efficiency and charge transfer efficiency, *ChemSusChem*, 2018, **11**(1), 276–284.

27 L. J. Zhang, T. F. Xie, D. J. Wang, *et al.*, Noble-metal-free CuS/CdS composites for photocatalytic H_2 evolution and its photogenerated charge transfer properties, *Int. J. Hydrogen Energy*, 2013, **38**(27), 11811–11817.

28 L. Zhang, T. Jiang, S. Li, *et al.*, Enhancement of photocatalytic H_2 evolution on $Zn_{0.8}Cd_{0.2}S$ loaded with CuS as cocatalyst and its photogenerated charge transfer properties, *Dalton Trans.*, 2013, **42**(36), 12998–13003.

29 L. J. Zhang, S. Li, B. K. Liu, *et al.*, Highly efficient CdS/WO_3 photocatalysts: Z-scheme photocatalytic mechanism for their enhanced photocatalytic H_2 evolution under visible light, *ACS Catal.*, 2014, **4**(10), 3724–3729.

30 P. A. Thiel and T. E. Madey, The interaction of water with solid surfaces: fundamental aspects, *Surf. Sci. Rep.*, 1987, **7**(6–8), 211–385.

31 R. Subbaraman, D. Tripkovic, D. Strmcnik, *et al.*, Enhancing hydrogen evolution activity in water splitting by tailoring Li^+-$Ni(OH)_2$-Pt interfaces, *Science*, 2011, **334**(6060), 1256–1260.

32 M. Gong, D. Y. Wang, C. C. Chen, *et al.*, A mini review on nickel-based electrocatalysts for alkaline hydrogen evolution reaction, *Nano Res.*, 2016, **9**(1), 28–46.